SLAM-based Joint Calibration of Differential RSS Sensor Array and Source Localization

Linya Fu*, Xu Qiao*, Shoudong Huang†, Guoqiang Mao‡, Zhiyun Lin*, Youfu Li§, and He Kong*¶
*Shenzhen Key Laboratory of Control Theory and Intelligent Systems, Southern Uni. of Sci. and Tech., Shenzhen, China; 12232297, 12232290@mail.sustech.edu.cn; linzy, kongh@sustech.edu.cn
†Robotics Institute, Uni. of Technology Sydney, Sydney, Australia; shoudong.huang@uts.edu.au
‡State Key Laboratory of Integrated Services Networks, Xidian University, China; gqmao@xidian.edu.cn
§ Department of Mechanical Engineering, City University of Hong Kong, China; meyfli@cityu.edu.hk
¶ Guangdong Provincial Key Laboratory of Human-Augmentation and Rehabilitation Robotics in Universities, Southern Uni. of Sci. and Tech., Shenzhen, China

IECON 2023- 49th Annual Conference of the IEEE Industrial Electronics Society | 979-8-3503-3182-0/23/$31.00 ©2023 IEEE | DOI: 10.1109/IECON51785.2023.10311803

***Abstract*—Sensor arrays generating differential received signal strength (DRSS) measurements have found many applications in robotics. However, accurate calibration of these sensor arrays remains a challenge. Most existing methods are impractical in that they assume to know signal source positions or certain parameters (i.e., path loss exponent), and try to estimate the others. In this paper, we adopt graph simultaneous localization and mapping (SLAM) as a general framework for jointly estimating the source positions and parameters of the DRSS sensor array. Our contributions are twofold. On the one hand, by using a Fisher information matrix approach, we conduct a systematic observability analysis of the corresponding SLAM setup for the calibration problem. On the other hand, we propose an effective procedure to select the initial value which is fed to Levenberg-Marquardt iterations for further improving optimization accuracy and convergence. Extensive simulation and hardware experiments show that the proposed method renders high-quality calibration results. All the codes and data are publicly available at https://github.com/SUSTech2022/DRSS-sensor-array-calibration.**

***Keywords*—RSS sensor array, SLAM, sensor calibration**

I. INTRODUCTION

Sensor array-based systems utilizing received signal strength (RSS) and differential RSS (DRSS) measurements can be employed in numerous robotic applications such as localization and tracking [1]-[3], navigation [4]-[5], mapping [6]-[7], multi-modal perception [8]-[10]. Accurate calibration of RSS/DRSS sensor arrays, as for other sensing modalities [11]-[16], is crucial for satisfactory performance. However, existing calibration methods for RSS/DRSS sensor arrays are impractical in that they either assume to know the signal source or the sensor positions or certain parameters (i.e., path loss exponent), and try to estimate the others. For example, by assuming to know the source positions, [17] proposed an iterative algorithm to estimate sensor locations and RSS model parameters. [18] proposed several techniques for estimating the path loss exponent (PLE) in the RSS model using power measurements and geometric constraints.

L. Fu and X. Qiao contributed equally to this work. This work was supported by the Science, Technology, and Innovation Commission of Shenzhen Municipality, China [Grant No. ZDSYS20220330161800001].

To our best knowledge, there is no existing work on joint calibration of the DRSS sensor array and source localization. The above problem can be conceptually considered as a standard SLAM problem [19]-[20], where the sensor array and the signal source act as features in the environment and the robot, respectively, and all measurements are used in the optimization as done in full information estimation [21]-[22]. Then, two important questions arise.

On the one hand, it is critical to assess whether the information included in the measurements is sufficient to estimate all the unknown variables. This is the so-called observability problem in the SLAM literature [23]-[26]. On the other hand, as with the standard graph SLAM, the considered calibration problem is a nonlinear least squares (LS) problem. Therefore, it is important to develop reliable calibration algorithms so that accurate parameter estimates can be obtained. However, many existing methods for solving the aforementioned nonlinear LS problems adopt Gauss-Newton types of iterations and require the initial value to be close to the true value (otherwise, the algorithm can lead to a local minimum or even diverge). This incurs significant difficulties in obtaining accurate estimates of the former calibration problem.

Motivated by the above observation, our major contributions in this paper are twofold. First, via a Fisher information matrix (FIM) approach [23]-[24], we conduct a systematic observability analysis of the corresponding SLAM setup for the calibration problem. Specifically, we establish necessary or sufficient conditions for the identifiability of unknown parameters. Second, we propose an effective procedure to select the initial value which is fed to Levenberg-Marquardt (LM) [27] iterations for further improving optimization accuracy and convergence. Extensive numerical simulations and hardware experiments show that the proposed method renders high-quality calibration results. Finally, as it is to be discussed later in the paper, given the nature of DRSS sensor models, calibration of the sensor array requires knowing the initial position of the signal source. This seems to be restrictive but can be handled in the calibration process by initializing the signal source at an approximately known position in a pre-defined global reference frame. **Notation**: $diag(\mathbf{A}, \mathbf{B})$ denotes

a block diagonal matrix with $\mathbf{A}$ and $\mathbf{B}$ being its block diagonal entries. $diag_n(\mathbf{A})$ denotes a block diagonal matrix with $\mathbf{A}$ as block diagonal entries for n times.

II. PRELIMINARIES AND PROBLEM STATEMENT

In a 3D calibration scenario with a sensor array containing N RSS sensors, there are consecutive signals emitted by a single signal source at K spatial positions. Denote the unknown positions of the i-th sensor and the source by $\mathbf{s}_i = [s_i^x, s_i^y, s_i^z]^{\mathrm{T}} \in \mathbb{R}^3$ and $\chi_k = [\chi_k^x, \chi_k^y, \chi_k^z]^{\mathrm{T}} \in \mathbb{R}^3$, respectively. The measurement of the i-th sensor is given by (in dB) [4]

$$P_i^k = P_0 - 10\gamma \log_{10} \frac{d_i^k}{d_0} + v_i, \tag{1}$$

where P_0 represents the unknown source transmit power at a reference distance d_0 (usually taken to be 1 m); d_i^k is the Euclidean distance between the i-th sensor and the source at time t_k ($k = 1, 2, \ldots, K$, where K is the total number of time steps); γ denotes the PLE; the term $v_i \sim \mathcal{N}(0, \sigma_i^2)$ represents the Gaussian noise (here we assume σ_i to be known).

If we select the first receiver as the reference sensor, i.e., $\mathbf{s}_1 = \mathbf{0}$, then (1) can be converted to the DRSS model:

$$P_{i1}^k = -10\gamma \log_{10} \left(\frac{d_i^k}{d_1^k} \right) + v_{i1}, \quad (i = 2, 3, \ldots, N) \tag{2}$$

where $v_{i1} = v_i - v_1 \sim \mathcal{N}(0, \sigma_i^2 + \sigma_1^2)$. Denote

$$\mathbf{s} = \left[(\mathbf{s}_2)^{\mathrm{T}}, (\mathbf{s}_3)^{\mathrm{T}}, \cdots, (\mathbf{s}_N)^{\mathrm{T}} \right]^{\mathrm{T}} \in \mathbb{R}^{3(N-1)}, \tag{3}$$

as the unknown states of the sensor array; and denote

$$\mathbf{x} = \left[\mathbf{s}^{\mathrm{T}}, (\chi_1)^{\mathrm{T}}, (\chi_2)^{\mathrm{T}}, \cdots, (\chi_K)^{\mathrm{T}}, \gamma \right]^{\mathrm{T}} \in \mathbb{R}^{3(N-1)+3K+1}, \tag{4}$$

as the whole unknown vectors to be identified. As shown in Fig. 1, the graph-based SLAM framework is a feasible solution to the above problems by treating the moving signal source as a robot and the sensor array as a single landmark (given that all sensors are "observed" at all times) [28].

For the position-position constraints, the measurement of the relative motion between positions k and $k+1$ ($k = 1, 2, \cdots, K-1$) can be expressed as

$$\mathbf{z}_{k,k+1}^{p-p} = \chi_{k+1} - \chi_k + \mathbf{w}_k, \tag{5}$$

where $\mathbf{w}_k \sim \mathcal{N}(\mathbf{0}, \mathbf{Q})$, and $\mathbf{Q} > \mathbf{0} \in \mathbb{R}^{3\times 3}$.

With regards to position-landmark constraints, the DRSS measurements related to each sensor when the source moves to the position at time step k can be defined as

$$\mathbf{z}_k^{p-l} = \left[P_{21}^k, P_{31}^k \ldots, P_{N1}^k \right]^{\mathrm{T}} \in \mathbb{R}^{N-1}. \tag{6}$$

From (2) we know that DRSS measurements $\mathbf{z}_k^{p-l}$ are subject to Gaussian noise $\mathbf{v} = [v_{21}, v_{31}, \cdots, v_{N1}]^{\mathrm{T}} \sim \mathcal{N}(\mathbf{0}, \mathbf{P})$, where $\mathbf{P} = diag(\sigma_2^2 + \sigma_1^2, \sigma_3^2 + \sigma_1^2, \cdots, \sigma_N^2 + \sigma_1^2)$. Therefore, the measurements can be combined as

$$\begin{aligned} \mathbf{z} &= \left[(\mathbf{z}_1^{p-l})^{\mathrm{T}}, (\mathbf{z}_{1,2}^{p-p})^{\mathrm{T}}, \cdots, (\mathbf{z}_{K-1,K}^{p-p})^{\mathrm{T}}, (\mathbf{z}_K^{p-l})^{\mathrm{T}} \right]^{\mathrm{T}} \\ &= \mathbf{g}(\mathbf{x}) + \lambda. \end{aligned} \tag{7}$$

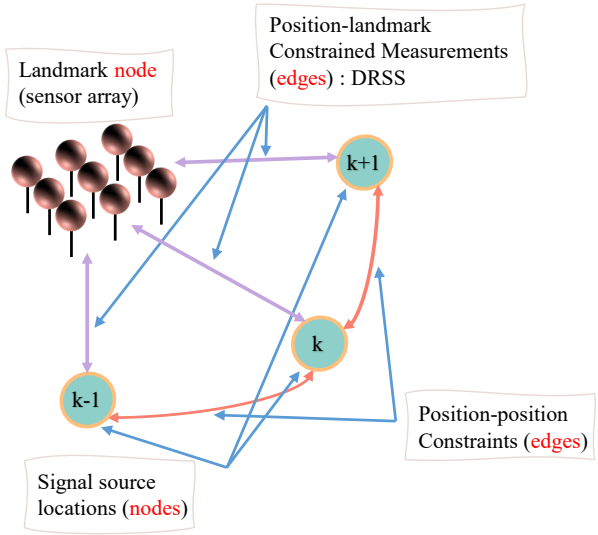

Fig. 1: Graph SLAM for joint source localization and DRSS sensor array calibration

where $\mathbf{g}(\mathbf{x})$ is the combined observation model, and $\lambda \sim \mathcal{N}(0, \mathbf{W})$ is the noise of the combined observations with the covariance matrix $\mathbf{W} = diag(diag_{K-1}(\mathbf{P}, \mathbf{Q}), \mathbf{P})$, therefore the information matrices of the whole observation can be written as $\Omega = \mathbf{W}^{-1}$. Define the error function as

$$\mathbf{e}(\mathbf{x}) = \widehat{\mathbf{z}}(\mathbf{x}) - \mathbf{z}, \tag{8}$$

where $\widehat{\mathbf{z}}(\mathbf{x})$ represents the estimates of $\mathbf{z}$. Then we have the objective function/cost function as

$$F(\mathbf{x}) = \mathbf{e}^{\mathrm{T}} \Omega \mathbf{e}. \tag{9}$$

As in [23]-[24], using graph SLAM, the joint calibration of the sensor array and source localization problem using DRSS measurements can be treated as the following standard least squares (LS) problem:

$$\mathbf{x}^* = \operatorname{argmin} F(\mathbf{x}). \tag{10}$$

The observability of SLAM is equivalent to the non-singularity of the FIM when described as a nonlinear LS parameter estimation problem [23]. The FIM of an unbiased estimator for the case of DRSS is defined as

$$\mathbf{I}_{FIM} \triangleq E\{[\nabla_{\mathbf{x}} ln\Lambda(\mathbf{x})][\nabla_{\mathbf{x}} ln\Lambda(\mathbf{x})]^{\mathrm{T}}\}, \tag{11}$$

where $\Lambda(\mathbf{x}) \triangleq p(\mathbf{z}|\mathbf{x})$ is the likelihood function, and the partial derivative should be calculated at the true value of $\mathbf{x}$ [29, chap. 2]. By following steps in [24] and [26], the FIM in (11) for models in (II) can be formulated as

$$\mathbf{I}_{FIM} = \mathbf{J}^{\mathrm{T}} \mathbf{W}^{-1} \mathbf{J}, \tag{12}$$

where $\mathbf{J}$ are the Jacobian matrix of the function $\mathbf{g}(\bullet)$ in (II) w.r.t. $\mathbf{x}$ [30, pp. 569], and will be discussed later in the paper (see in (18)). When $\mathbf{W} > 0$, we have $rank(\mathbf{J}) = rank(\mathbf{I}_{FIM})$.

If an initial value $\mathbf{x}_0$ is given, the numerical solution of (10) can be obtained by using the popular GN or LM algorithms. The idea is to approximate the cost function by its first-order Taylor expansion around $\mathbf{x}_0$:

$$\mathbf{e}(\mathbf{x}_0+\Delta\mathbf{x}) \approx l(\Delta\mathbf{x}) \equiv \mathbf{e}(\mathbf{x}_0)+\mathbf{J}\Delta\mathbf{x}, \tag{13}$$

where $\mathbf{J}$ is the Jacobian of $\mathbf{e}(\mathbf{x})$ computed in $\mathbf{x}_0$, and has the same form as in (18). Substituting (13) into (10) yields:

$$\begin{array}{l} F(\mathbf{x}_0+\Delta\mathbf{x}) \approx L(\Delta\mathbf{x}) \equiv [l(\Delta\mathbf{x})]^{\mathrm{T}}\Omega l(\Delta\mathbf{x}) \\ = F(x)+2\mathbf{e}^T\Omega\mathbf{J}\Delta\mathbf{x}+\Delta\mathbf{x}^T\mathbf{J}^T\Omega\mathbf{J}\Delta\mathbf{x}. \end{array} \tag{14}$$

Let $\mathbf{L}'(\Delta\mathbf{x})=0$, we have:

$$\mathbf{H}\Delta\mathbf{x}=-\mathbf{b}. \tag{15}$$

where $\mathbf{H}=\mathbf{J}^T\Omega\mathbf{J}$, and $\mathbf{b}=\mathbf{e}^T\Omega\mathbf{J}$. Therefore the iteration step size $\Delta\mathbf{x}$ can be obtained by solving Eq. (15). However, $\mathbf{H}$ is usually semi-positive definite, so the GN method cannot guarantee the convergence of the iterations. To address this issue, the LM method introduces a damping factor $\mu>0$

$$(\mathbf{H}+\mu\mathbf{I})\Delta\mathbf{x}=-\mathbf{b}. \tag{16}$$

to ensure $\mathbf{H}+\mu\mathbf{I}>0$. Note that convergence and accuracy of GN or LM methods largely depend on whether the initial value is close to the true value.

Problem statement: (1) find conditions whether and under which the FIM associated with the DRSS[1] measurements, i.e., $\mathbf{I}_{FIM}$ in (12) is non-singular, or equivalently, the Jacobian matrix $\mathbf{J}$ has full column rank; (2) design an efficient initial value selection framework and calibration algorithm to solve the nonlinear LS (10).

III. MAIN RESULTS

A. Observability Analysis

For the DRSS measurement model, the first sensor is considered as a reference, its relevant variables are all assumed to be zero and are excluded from the observability analysis. Thus, we have $\mathbf{J}\in\mathbb{R}^{n_1\times n_2}$, with $n_1=(N-1)K+3(K-1),\ n_2=3(N-1)+3K+1$, where n_1 and n_2 are the numbers of measurements and unknown variables, respectively. For $\mathbf{J}$ to be of full column rank, it is necessary that

$$n_1\geq n_2 \Longrightarrow K\geq\frac{4}{N-1}+3. \tag{17}$$

Proposition 1. *For the case of DRSS measurements, the Jacobian matrix can be written as*

$$\mathbf{J}=\underbrace{\begin{bmatrix} \mathbf{L}_1 & \mathbf{T}_1 & \mathbf{0}_{\widetilde{N}\times 3} & \cdots & \mathbf{0} & \mathbf{0} & \mathbf{B}_1 \\ \mathbf{0}_{3\times 3\widetilde{N}} & -\mathbf{I}_3 & \mathbf{I}_3 & \cdots & \mathbf{0} & \mathbf{0} & \mathbf{0}_{\widetilde{N}\times 1} \\ \vdots & \vdots & \vdots & \ddots & \vdots & \vdots & \vdots \\ \mathbf{L}_{K-1} & \mathbf{0} & \mathbf{0} & \cdots & \mathbf{T}_{K-1} & \mathbf{0} & \mathbf{B}_{K-1} \\ \mathbf{0} & \mathbf{0} & \mathbf{0} & \cdots & -\mathbf{I}_3 & \mathbf{I}_3 & \mathbf{0} \\ \mathbf{L}_K & \mathbf{0} & \mathbf{0} & \cdots & \mathbf{0} & \mathbf{T}_K & \mathbf{B}_K \end{bmatrix}}_{\mathbf{J}_1 \qquad \mathbf{J}_2=[\mathbf{J}_{21},\mathbf{J}_{22},\cdots,\mathbf{J}_{2K}] \qquad \mathbf{J}_3}, \tag{18}$$

where $\widetilde{N}=N-1$, and expressions of $\mathbf{L}_k$,$\mathbf{T}_k$ and $\mathbf{B}_k$ (for $k=1,2,...,K$) can be found in (23)-(28).

Proof. First, from (5) we notice that the corresponding Jacobian matrices are $\frac{\partial\chi_{k-1}^{\Delta}}{\chi_{k-1}}=-\mathbf{I}$, $\frac{\partial\chi_{k-1}^{\Delta}}{\chi_k}=\mathbf{I}$. Second, for $i=1,2,...,N$, the distance between the i-th sensor and the source at time instance t_k is

$$d_i^k=\sqrt{(\Delta x_{i\_k})^2+(\Delta y_{i\_k})^2+(\Delta z_{i\_k})^2}, \tag{19}$$

where

$$\Delta x_{i\_k}=\chi_k^x-s_i^x,\ \Delta y_{i\_k}=\chi_k^y-s_i^y,\ \Delta z_{i\_k}=\chi_k^z-s_i^z. \tag{20}$$

Based on (2) and (6), we have

$$\mathbf{z}_k=-10\gamma\begin{bmatrix} \log_{10}\frac{d_2^k}{d_1^k} & \cdots & \log_{10}\frac{d_N^k}{d_1^k} \end{bmatrix}^{\mathrm{T}}+\begin{bmatrix} v_{21} \\ \vdots \\ v_{N1} \end{bmatrix}, \tag{21}$$

with d_i^k as given in (19), for $i=2,3,...,N$, and

$$d_1^k=\sqrt{(\chi_k^x)^2+(\chi_k^y)^2+(\chi_k^z)^2}, \tag{22}$$

is the distance from the source position at the k-th time instance to the origin. Based on (3) and (21), we have

$$\mathbf{L}_k=\frac{\partial\mathbf{z}_k}{\partial\mathbf{s}}=\begin{bmatrix} \mathbf{J}_2^k & \mathbf{J}_3^k & \cdots & \mathbf{J}_N^k \end{bmatrix}\in\mathbb{R}^{\widetilde{N}\times 3\widetilde{N}}, \tag{23}$$

where for $i=2,3,...,N$, $\mathbf{J}_i^k\in\mathbb{R}^{N\times 3}$, and only entries of $\mathbf{J}_i^k$ on its $(i-1)$th row are nonzero, i.e.,

$$\mathbf{D}_i^k=\mathbf{J}_i^k(i-1:)=\mathbf{u}_k^i\in\mathbb{R}^{1\times 3}\ , \tag{24}$$

with $\mathbf{u}_k^i$ defined in (26). We also have

$$\begin{array}{l} \mathbf{T}_k=\frac{\partial\mathbf{z}_k}{\partial\chi_k}=\begin{bmatrix} \mathbf{J}_{k\_x} & \mathbf{J}_{k\_y} & \mathbf{J}_{k\_z} \end{bmatrix} \\ =-\left[\mathbf{u}_k^2,\mathbf{u}_k^3,\cdots,\mathbf{u}_k^N\right]^{\mathrm{T}}+\left[\mathbf{v}_k,\mathbf{v}_k,\cdots,\mathbf{v}_k\right]^{\mathrm{T}}\in\mathbb{R}^{\widetilde{N}\times 3}, \end{array} \tag{25}$$

with

$$\mathbf{u}_k^i=\left[\frac{10\gamma\Delta x_{i\_k}}{\left(d_i^k\right)^2\ln 10},\frac{10\gamma\Delta y_{i\_k}}{\left(d_i^k\right)^2\ln 10},\frac{10\gamma\Delta z_{i\_k}}{\left(d_i^k\right)^2\ln 10}\right], \tag{26}$$

$$\mathbf{v}_k=\left[\frac{10\gamma\chi_k^x}{\left(d_1^k\right)^2\ln 10},\frac{10\gamma\chi_k^y}{\left(d_1^k\right)^2\ln 10},\frac{10\gamma\chi_k^z}{\left(d_1^k\right)^2\ln 10}\right], \tag{27}$$

and

$$\mathbf{B}_k=\frac{\partial\mathbf{z}_k}{\partial\gamma}=-10\begin{bmatrix} \log_{10}\frac{d_2^k}{d_1^k} & \cdots & \log_{10}\frac{d_N^k}{d_1^k} \end{bmatrix}^{\mathrm{T}}\in\mathbb{R}^{\widetilde{N}\times 1}. \tag{28}$$

The results follow from the definition of the Jacobian [30, pp. 569]. □

[1]Our investigation shows that the SLAM problem associated with the RSS model (see Eq. (1)) is not observable within the FIM framework, so we focus on the DRSS case.

Lemma 1. *The Jacobian matrix* $\mathbf{J}$ *in (18) is of full column rank if and only if*

$$\mathbf{F} = \underbrace{\begin{bmatrix} \mathbf{L}_1 & \mathbf{T}_1 & \mathbf{B}_1 \\ \mathbf{L}_2 & \mathbf{T}_2 & \mathbf{B}_2 \\ \vdots & \vdots & \vdots \\ \mathbf{L}_K & \mathbf{T}_K & \mathbf{B}_K \end{bmatrix}}_{\mathbf{L}\quad\mathbf{T}\quad\mathbf{B}}, \tag{29}$$

is of full column rank.

Proof. The proof follows from [23] and is skipped here. □

Theorem 1. *The Jacobian matrix* $\mathbf{J}$ *in (18) is of full column rank only if both the following statements hold true:*

(i) For every sensor, i.e., $i = 2, 3, \cdots, N$*, there exist at least three time steps,* $1 \leq k_i^s \leq K$*, with* K *satisfying (17) and* $1 \leq s \leq 3$*, such that*

$$\mathbf{G}_i = \left[\mathbf{D}_i^{k_i^1}, \mathbf{D}_i^{k_i^2}, \mathbf{D}_i^{k_i^3}\right], \tag{30}$$

with $\mathbf{D}_i^{k_i^s}$ *defined in (24), is of full column rank;*

(ii) There exist $r_1, r_2, r_3 (2 \leq r_1, r_2, r_3 \leq N)$ *(any two or all of* r_1, r_2, r_3 *can be equal, or they can be all different) and at least three time instances*[2] $k_1, k_2, k_3 (1 \leq k_1, k_2, k_3 \leq K)$*, out of* K *time steps (with* K *satisfying (17)), such that the matrix*[3]

$$\mathbf{O}_r = \left[\mathbf{O}_{r_1}^{k_1}, \mathbf{O}_{r_2}^{k_2}, \mathbf{O}_{r_3}^{k_3}\right], \tag{31}$$

is of full column rank, where $\mathbf{O}_i^k = -\mathbf{u}_k^i + \mathbf{v}_k$*, with* $\mathbf{u}_k^i$ *and* $\mathbf{v}_k$ *defined in in (26) and (27).*

Proof. From Lemma 1, we know that $\mathbf{J}$ has full column rank if and only if $\mathbf{F}$ has full column rank. For $\mathbf{F}$ to have full rank, $\mathbf{L}$, $\mathbf{T}$ and $\mathbf{B}$ in (29) have to be of full column rank.

(i) Note that from (24) and (23), $\mathbf{L}_k$ can be expressed as $\mathbf{L}_k = diag(\mathbf{D}_2^k, \mathbf{D}_3^k, \cdots, \mathbf{D}_{N-1}^k, \mathbf{D}_N^k)$. By omitting the zero blocks in $\mathbf{J}_1$, one has that

$$\overline{\mathbf{J}}_1 = \begin{bmatrix} diag(\mathbf{D}_2^1, \mathbf{D}_3^1, \cdots, \mathbf{D}_{N-1}^1, \mathbf{D}_N^1) \\ diag(\mathbf{D}_2^2, \mathbf{D}_3^2, \cdots, \mathbf{D}_{N-1}^2, \mathbf{D}_N^2) \\ \vdots \\ diag(\mathbf{D}_2^K, \mathbf{D}_3^K, \cdots, \mathbf{D}_{N-1}^K, \mathbf{D}_N^K) \end{bmatrix},$$

and denote each column in $\overline{\mathbf{J}}_1$ as $\mathbf{J}_{1i} \in \mathbb{R}^{K(N-1)\times 3}$, for $i = 2, 3, ..., N$. Moreover, it holds that $rank(\mathbf{J}_1) = rank(\overline{\mathbf{J}}_1)$. Also, since the columns of $\mathbf{J}_{1i}$ are independent of each other, the full column rank of $\overline{\mathbf{J}}_1$ (and $\mathbf{J}_1$) is equivalent to the full column rank of $\mathbf{J}_{1i} \in \mathbb{R}^{K(N-1)\times 3}$, for $i = 2, 3, ..., N$. Note $\mathbf{J}_{1i}$ has full rank if and only there exist at least four time steps, $1 \leq k_i^s \leq K$, with K satisfying (17) and $1 \leq s \leq 3$, such that $\mathbf{G}_i$ in (30) has full column rank.

(ii) $\mathbf{T}$ in (29) is of full column rank only if a 3×3 matrix formed by at least one of the 3-permutation of its rows is of full rank. From the expressions of $\mathbf{T}_k$ in (25), if $k_1 = k_2 = k_3$ ($r_1 = r_2 = r_3$), one must have that $r_1 \neq r_2 \neq r_3$ ($k_1 \neq k_2 \neq k_3$), for $\mathbf{O}_r$ to have full rank. Similarly, if $k_i = k_j$ and $r_i = r_j$, it is impossible for $\mathbf{O}_r$ to be of full rank. The above arguments lead to the statements in part (ii). □

Note that the four time steps necessary for condition (30) to hold may vary depending on the sensor. Also, Theorem 1 reveals whether condition (29) (or conditions (30)-(31)) holds relies on the sensor array configuration and the source trajectory (i.e., $\mathbf{s}_i$ and $\chi_{\mathbf{k}}$). This naturally raises the question of at what sensor array setup and source trajectory the observability of the whole system is impossible. We will state our findings in the following theorem.

Theorem 2. *The following statements hold true:*

(i) If all sensors (except the first one which is set as the reference) locate on the surface of the same sphere $(x-a)^2 + (y-b)^2 + (z-c)^2 = r^2$ *where* a, b, c *and* r *take any real numbers, and for* $k = 1, 2, \cdots, K$*, the source is static and located at the sphere centre, then it is impossible for* $\mathbf{F}$ *in (29) to have full column rank.*

(ii) For $k = 1, 2, \cdots, K$*, if the trajectory of the source is always in the same plane* $y = \alpha x, z = \beta y$ *or* $x = \theta z$ *as all sensors, where* α, β *and* θ *takes any real number, then it is impossible for* $\mathbf{L}$ *and* $\mathbf{T}$ *in (29) to have full column rank.*

(iii) If either of (i) or (ii) occurs, the Jacobian matrix $\mathbf{J}$ *will not be of full column rank, which leads to an unobservable SLAM problem.*

Proof. (i) When all sensors (except the first one) are on the surface of sphere $(x-a)^2 + (y-b)^2 + (z-c)^2 = r^2$, we have $\chi_k = [a, b, c]$, $d_1^k = d_1 = constant$, $d_2^k = d_3^k = \cdots = d_N^k = r$, so that

$$\begin{aligned} \mathbf{T}' &= \mathbf{L}_{1,3} + \mathbf{L}_{4,6} + \cdots + \mathbf{L}_{3\widetilde{N}-2,3\widetilde{N}} + \mathbf{T} \\ &= \frac{10\gamma}{(d_1)^2 \ln 10} \begin{bmatrix} a, b, c \\ \vdots \\ a, b, c \end{bmatrix}, \end{aligned}$$

where $\mathbf{L}_{i,j}$ denotes the i^{th} to j^{th} columns of $\mathbf{L}$. It is clear that $\mathbf{T}'$ is not of full column rank. Hence, it is impossible for $\mathbf{F}$ to have full column rank.

(ii) Without loss of generality, assume the source trajectory and $\mathbf{s}_i$ are in the plane $y = \alpha x$, that is $\chi_k^y = \alpha \chi_k^x$, $\mathbf{s}_i^y = \alpha \mathbf{s}_i^x$ so we have $\Delta y_{i\_k} = \alpha \Delta x_{i\_k}$, with Δx_{i_k} and Δy_{i_k} defined in (20). Thus, it leads to the non-full column rank of $\mathbf{L}$ and $\mathbf{T}$.

(iii) This part follows from the fact that if $\mathbf{F}$ is not of full rank, then $\mathbf{J}$ loses rank either. This completes the proof. □

B. Joint Estimation Algorithm

We set the coordinate frame as follows: Let the position of the first sensor be the coordinate origin, the second sensor be on the positive half-axis of the X-axis, and the plane where the first three sensors locate be the XOY plane. Therefore, once the positive direction of the Z-axis is determined, the coordinate system is determined as well.

[2]Here we use time instances, instead of time steps, to incorporate the possibilities that any two or all the three of k_1, k_2, k_3 might be equal.

[3]Note that by writing O_r as in (31), we implicitly exclude the cases where $k_i = k_j$ and $r_i = r_j$, because under such conditions, it is impossible for O_r to have full column rank.

*1) **Selection of Initial Value**:* Since the performance of the GN method is sensitive to the initial value, it is important to come up with a reliable initialization procedure. As for a standard SLAM problem [24], here for the joint calibration of DRSS sensor array and source localization, all the measurements in (II) only contain information about either the relative positions of the signal source or between the source and the sensor array. Hence, the initial source position w.r.t. an arbitrary global coordinate frame is not observable. As in SLAM, this issue is typically addressed by placing the origin of the global coordinate frame at the initial source position. For calibration purposes, we cannot do this (since the origin is taken to be the first sensor position). However, we can initialize the source at a position that is approximately known w.r.t. the origin. Hence, we assume a good guess of the initial position of the signal source $\widehat{\chi}_1$. Also, based on engineering experience [18], [31]-[32], the value of the PLE γ lies in the interval $[1, 7]$, which we take as prior information. However, its true value is not assumed to be known. For initialization, we randomly select the value of γ from the interval $[1, 7]$. Thus, our proposed initial value estimation framework is described as follows:

(i) Estimation of the initial value of the signal source positions: By combining the relative position measurements $\mathbf{z}_{k,k+1}^{p-p}$ with the approximate initial position of the source $\widehat{\chi}_1$, we can estimate the trajectory of the signal source. More specifically, the signal source positions can be estimated as:

$$\widehat{\chi}_{k+1} = \widehat{\chi}_k + \mathbf{z}_{k,k+1}^{p-p}, \tag{32}$$

where $k = 1, 2, \cdots, K-1$.

(ii) Estimation of the initial value of the sensor positions: We use the spatial four-point localization method [33] to solve for the initial sensor array positions. This method requires four known source positions in space so that several equations can be constructed using the constraints in spatial geometry to solve for the coordinates of one particular unknown point (i.e., an unknown sensor location).

Assume $\widehat{\chi}_{k_j}$ $(j = 1, 2, 3, 4,\ k_j = 1, 2, \cdots, K)$ are the coordinates of four known signal positions obtained from step (i), $\mathbf{s}_i$ $(i = 2, 3, \cdots, N-1)$ are the coordinates of the unknown sensor to be solved, and $d_i^{k_j}$ is the distance between $\widehat{\chi}_{k_j}$ and $\mathbf{s}_i$. Based on 3D geometry, we have:

$$\begin{cases} \left(\widehat{\chi}_{k_1}^x - s_i^x\right)^2 + \left(\widehat{\chi}_{k_1}^y - s_i^y\right)^2 + \left(\widehat{\chi}_{k_1}^z - s_i^z\right)^2 = (d_i^{k_1})^2 \\ \left(\widehat{\chi}_{k_2}^x - s_i^x\right)^2 + \left(\widehat{\chi}_{k_2}^y - s_i^y\right)^2 + \left(\widehat{\chi}_{k_2}^z - s_i^z\right)^2 = (d_i^{k_2})^2 \\ \left(\widehat{\chi}_{k_3}^x - s_i^x\right)^2 + \left(\widehat{\chi}_{k_3}^y - s_i^y\right)^2 + \left(\widehat{\chi}_{k_3}^z - s_i^z\right)^2 = (d_i^{k_3})^2 \\ \left(\widehat{\chi}_{k_4}^x - s_i^x\right)^2 + \left(\widehat{\chi}_{k_4}^y - s_i^y\right)^2 + \left(\widehat{\chi}_{k_4}^z - s_i^z\right)^2 = (d_i^{k_4})^2 \end{cases}. \tag{33}$$

For $d_i^{k_j}$ in (33), we can estimate its value based on the DRSS model (2) as $d_i^{k_j} = d_1^{k_j} 10^{m_i^k}$, where $m_i^k = P_{i1}^{k_j}/(-10\gamma_i)$. After eliminating some squared terms, (33) can be simplified and rewritten in the following matrix form

$$\mathbf{M}\mathbf{c} = \mathbf{d}, \tag{34}$$

where $\mathbf{c} = [s_i^x, s_i^y, s_i^z]^{\mathrm{T}}$ is the position of sensor i to be estimated, and detailed expressions of $\mathbf{M}$ and $\mathbf{d}$ are skipped here due to limited space. Note that Eq. (34) has a unique solution as long as the matrix $\mathbf{M}$ is of full rank, i.e., the four points chosen are not coplanar.

*2) **Algorithm Implementation**:* The algorithm flow of joint calibration of the DRSS sensor array and source localization is shown in Algorithm 1. Note in step 12 of Algorithm 1, we set an upper error limit lim to discard bad initial values. Given $K \gg 4$, so one can continuously re-select four points $\widehat{\chi}_{k_j}$ to improve initial value calculation until $F(\mathbf{x}_0) < lim$. For the calibration task after the initial value selection procedure, we choose the LM method to improve convergence and estimation accuracy. Finally, the parameter estimates are saved to g_{est} and returned by the algorithm.

Algorithm 1 Joint Calibration of the DRSS Sensor Array and Source Localization

Input: initial graph g_{raw} (includes initial value $\mathbf{x}_0$)
Output: estimated graph g_{est} (includes final estimate $\widehat{\mathbf{x}}$)

1: $g_0 = g_{raw}$
2: $g_0.gamma = random([1, 7])$
3: $\widehat{\chi}_1 = [x_0, y_0, z_0]^{\mathrm{T}}$ // initial position of the signal source
4: **for** $k = 1 : K-1$ **do**
5: $\quad \widehat{\chi}_{k+1} = \widehat{\chi}_k + \mathbf{z}_{k,k+1}^{p-p}$ // Eq. (32)
6: **end for**
7: $g_0.source = [\widehat{\chi_1}, \widehat{\chi_2}, \cdots, \widehat{\chi}_K]^{\mathrm{T}}$
8: $g_0.sensor_1 = [0, 0, 0]^{\mathrm{T}}$ //fix the reference sensor
9: $[g_0.sensor_2, \cdots, g_0.sensor_N] = SensorInit(g)$// Eq. (34)
10: $g_1 = LM(g_0)$ //iterate using LM method
11: $cost = computeGlobalError(g_1)$ // cost function
12: **while** $cost > lim$ **do**
13: $\quad [g_0.sensor_2, \cdots, g_0.sensor_N] = SensorInit(g)$
14: $\quad g_1 = LM(g_0)$
15: $\quad cost = computeGlobalError(g1)$
16: **end while**
17: $g_{est} = g_1$
18: **return** g_{est}

IV. NUMERICAL SIMULATIONS

A. Observability Verification

We design a sensor array with 8 sensors and two source trajectories with $K = 80$ or 49 to simulate some cases with DRSS measurements where observability is guaranteed, as shown in Fig. 2. For trajectory 1, following Theorem 1, we select $k_2^1 = 9$, $k_2^2 = 14$, $k_2^3 = 23$, then $\mathbf{G}_i$ in (30) becomes

$$\mathbf{G}_2 = \begin{bmatrix} -19.7407 & 7.8963 & -7.8963 \\ -5.3543 & 14.2782 & 0 \\ 15.6346 & 0 & 20.8461 \end{bmatrix},$$

with $rank(\mathbf{G}_2) = 3$, i.e., it has full column rank. If we select $r_1 = 4$, $r_2 = 6$, $r_3 = 6$, and $k_1 = 7$, $k_2 = 7$, $k_3 = 9$, so that $\mathbf{O}_r$ in (31) becomes

$$\mathbf{O}_r = \begin{bmatrix} 3.4068 & -20.8795 & -29.2314 \\ 3.4068 & -29.2314 & -20.8795 \\ 3.4068 & 29.2314 & -20.8795 \end{bmatrix},$$

with $rank(\mathbf{O}_r) = 3$, which means $\mathbf{O}_r$ has full column rank. We also verify that $\mathbf{F}$ in (29), of dimension 797×25, is of full column rank. Furthermore, we have the Jacobian matrix $\mathbf{J}$ in (18), which is a 797×262 matrix and has full column rank. Therefore, the system is observable. To double confirm, we run Algorithm 1. As can be seen in Fig. 2(b), the estimated sensor array and signal source locations have converged close to their corresponding ground truth locations. We can also perform similar validations for trajectory 2. We also simulate the unobservable cases in Theorem 2 and verify that $\mathbf{F}$ is not of full column rank, and the algorithm fails to find the solution to the LS in (10). Details are skipped here.

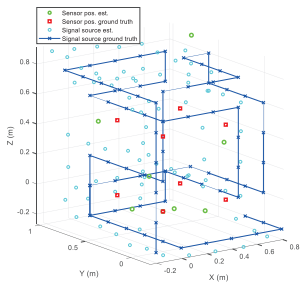

(a) Trajectory 1: initial guess g_0

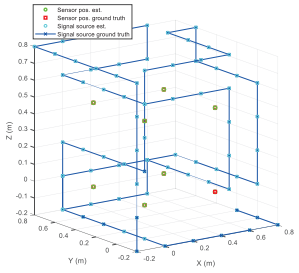

(b) Trajectory 1: estimated results g_{est}

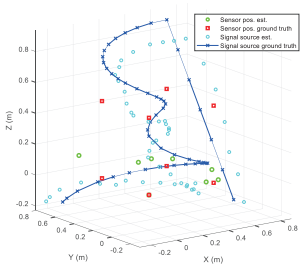

(c) Trajectory 2: initial guess g_0

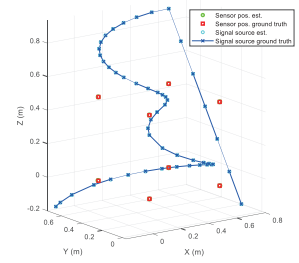

(d) Trajectory 2: estimated results g_{est}

Fig. 2: Simulation estimates of two kinds of trajectories: segmented linear (trajectory 1) and non-linear (trajectory 2).

B. Algorithm Error Analysis

We analyzed the estimation error for each trajectory using the root mean square error (RMSE). Table I shows the average RMSEs for 50 runs of the algorithm using different initial values: $Lv1$ and $Lv2$ are obtained by adding Gaussian noise to the ground truth values, while $ours$ uses our initial value selection method. The results show that our method achieves similar RMSEs to those using ground truth plus noise, without relying on true values for initialization. We also found that calibration results using segmented linear trajectories are significantly better than those using nonlinear trajectories. Fig. 2 confirms the validity of the algorithm.

TABLE I: Average RMSE of estimated parameters*

	Trajectory 1 (segmented linear)			Trajectory 2 (non-linear)		
Noise Level	χ	$\mathbf{s}$	γ	χ	$\mathbf{s}$	γ
$Lv1$	0.00012	0.00012	0.00157	0.00123	0.00114	0.00905
$Lv2$	0.00014	0.00014	0.00180	0.00164	0.00155	0.01190
$Ours$	0.00015	0.00014	0.00191	0.00539	0.00521	0.05096

* Note: χ denotes source positions of all time steps, $\mathbf{s}$ denotes positions of the sensor array, and γ denotes the PLE. The unit of χ and $\mathbf{s}$ in the table is meter.

V. EXPERIMENTS

A. Experimental Environment Configuration

The experimental site was carefully selected to minimize measurement error. The site chosen was an open laboratory measuring $9.1m \times 14.4m \times 3.6m$. As depicted in Fig. 3, the experiment was conducted on a flat surface measuring $1.2m \times 1.2m$, with the floor grid serving as the unit of measurement.

For the selection of the initial value of γ, we calculated from several experimental data that γ falls roughly on the interval $[2, 3]$ according to

$$\gamma \approx \frac{P_{i1}^k}{-10 \log_{10}\left(\frac{d_i^k}{d_1^k}\right)}$$

To facilitate the estimation of the RMSE, we take the true value of γ as 2.5. In this experiment, we utilized a total of five ZigBee units capable of transmitting and receiving RSS signals. One unit was designated as the router and served as the signal-transmitting source in the ZigBee network. The remaining four units were designated as terminals and served as signal receivers to measure the value of the DRSS. The Cartesian coordinate system was established with the antenna base of sensor 1 as the reference node, the X-axis (blue line) in the transverse direction, and the Y-axis (green line) in the longitudinal direction, as shown in Fig. 3. The four sensors were positioned at the vertices of a rectangle on the measuring unit, with coordinates sensor $1 = [0.0, 0.0, 0.0]^{\mathrm{T}}$, sensor $2 = [1.2, 0.0, 0.0]^{\mathrm{T}}$, sensor $3 = [0.0, 1.2, 0.0]^{\mathrm{T}}$, sensor $4 = [1.2, 1.2, 0.0]^{\mathrm{T}}$. The signal source originated from $[0.2, 0.0, 0.0]^{\mathrm{T}}$ and its trajectory is depicted in Fig. 5(a). Each step advanced 0.2m in one direction, and RSS data of four sensors for $K = 74$ were recorded.

B. Analysis of Experimental Results

To evaluate the effectiveness of our proposed joint calibration and localization algorithm (Algorithm 1), we input the collected trajectory data and run each trajectory 80 times to obtain 80 independent sets of estimates. We then calculate the mean of the estimates obtained from 10, 20, ..., up to 80 sets, respectively, and record the corresponding RMSEs. We also generate boxplots to visualize the distribution of the RMSE values.

To enhance the precision of our estimates and mitigate the influence of outliers, we employed two commonly used statistical techniques, namely the σ rule and the interquartile range (IQR) method. We evaluated the effect of outlier processing

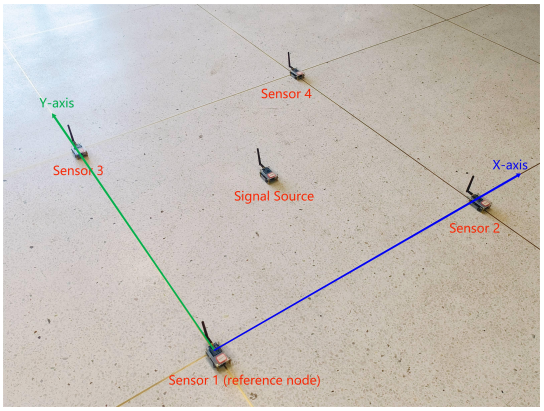

Fig. 3: Experiment Setup

by recalculating the RMSEs of the mean estimates before and after processing, as depicted in Fig. 4. The results show that the mean RMSEs of both the source and the sensor array estimates decrease gradually with an increasing number of estimated data sets, indicating an improvement in estimate accuracy. However, we also noticed that the RMSEs start to increase beyond a certain number of data points (around 50), suggesting that collecting more data may not significantly impact the results. Therefore, we conclude that 50 sets of data may be sufficient for our proposed joint calibration and localization algorithm. Without loss of generality, we take 30 sets of estimates for analysis. Fig. 5 presents the initial values of the algorithm, which are different for each run and have been averaged for presentation, as well as the estimation results obtained after processing these 30 sets of estimates using the IQR method. And Fig. 6 shows the boxplots of RMSEs of these 30 sets of estimates before and after data processing. The corresponding RMSEs for the signal source and the sensor array are 0.0864m and 0.0678m, respectively. The average PLE is 2.9109.

It should be noted that the experimental RMSE values were observed to be higher compared to the simulated results. This disparity can be attributed to several factors. For example, in the actual experiments, the DRSS model's PLE was not constant and exhibited significant spatial variations due to the non-coplanar configuration of the signal source trajectory and the sensor array. This deviation from the simulated assumption of a constant PLE model led to increased fluctuations in the measured DRSS values. Additionally, the presence of noises in the experiments further impacted the performance of the calibration algorithm. While we approximated the noise values in the simulation based on empirical assumptions, the actual noise magnitude in the experiments remained unknown, contributing to the observed differences between the experimental and simulated RMSE values.

Despite these challenges, our method shows promise in calibrating and localizing DRSS sensor arrays. Further investigations and improvements, particularly addressing the varying PLE and noise factors, are planned as part of future work to enhance the applicability of our algorithm in complex 3D scenarios. We also plan to extend the experimental design to investigate cases with larger sensor array spacing, aiming to gain a more comprehensive understanding of the relationship between the calibration error and the size of the sensor array.

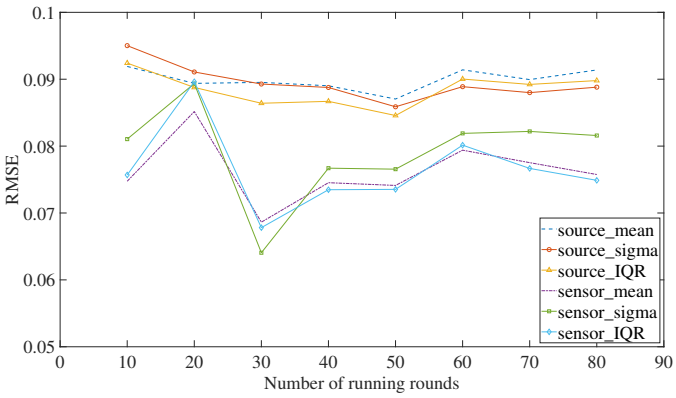

Fig. 4: The RMSEs corresponding to the mean of 8 groups of estimates

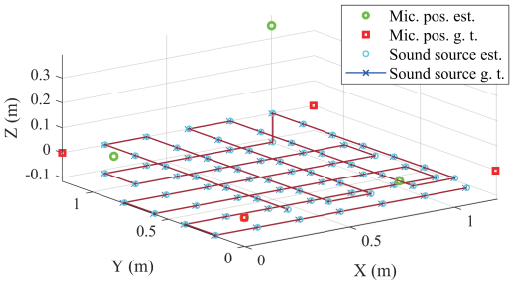

(a) Mean initial value

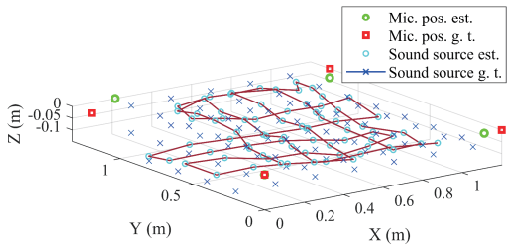

(b) Estimated results

Fig. 5: Initial values and estimated results

VI. CONCLUSIONS

This paper presents a joint calibration method for DRSS sensor arrays and source localization using graph SLAM. Our contributions are twofold: First, we conducted a systematic observability analysis of the SLAM setup for the calibration problem using a FIM approach. Second, we proposed an effective procedure for selecting initial values for LM iterations to improve optimization accuracy and convergence. Numerical simulations demonstrate that our method produces comparable calibration results when compared to scenarios that use noise-corrupted ground truth values as initial values.

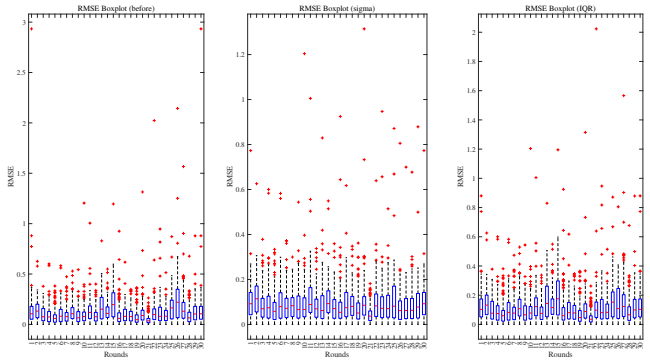

Fig. 6: Boxplots of RMSEs of 30 sets of estimates before and after data processing.

Some preliminary real experiments further verify the effectiveness of our algorithm. Future work will aim to enhance the method's applicability in more complex 3D scenarios and reduce the disparities observed between experimental results and simulations.

VII. ACKNOWLEDGMENT

The authors are grateful to Dr. Kaide Huang of Foshan University for his helpful discussions.

REFERENCES

[1] Y. Guo, K. Huang, N. Jiang, X. Guo, Y. Li, and G. Wang, An exponential-rayleigh model for RSS-based device-free localization and tracking, *IEEE Transactions on Mobile Computing*, Vol. 14, No. 3, pp. 484–494, 2015.

[11] J. Zhang, Q. Lyu, G. Peng, Z. Wu, Q. Yan, and D. Wang, LB-L2L-Calib: Accurate and robust extrinsic calibration for multiple 3D LiDARs with long baseline and large viewpoint difference, *Proceeding of the IEEE International Conference on Robotics and Automation (ICRA)*, Vol. 22, No. 11, pp. 926–932, 2022.

[2] J. N. Twigg, J. R. Fink, P. L. Yu, and B. M. Sadler, RSS gradient-assisted frontier exploration and radio source localization, *Proceedings of the IEEE International Conference on Robotics and Automation (ICRA)*, pp. 889–895, 2012.

[3] W. A. Zhang, X. Yang, L. Yu, and S. Liu, Sequential fusion estimation for RSS-based mobile robots localization with event-driven WSNs, *IEEE Transactions on Industrial Informatics*, Vol. 12, No. 4, pp. 1519–1528, 2016.

[4] N. Deshpande, E. Grant, T. C. Henderson, and M. T. Draelos, Autonomous navigation using received signal strength and bearing-only pseudogradient interpolation, *Robotics and Autonomous Systems*, Vol. 75, pp. 129–144, 2016.

[5] A. Achroufene, Y. Amirat, and A. Chibani, RSS-based indoor localization using belief function theory, *IEEE Transactions on Automation Science and Engineering*, Vol. 16, No. 3, pp. 1163–1180, 2019.

[6] K. Kotay, R. Peterson, and D. Rus, Experiments with robots and sensor networks for mapping and navigation, *Field and Service Robotics*, Vol. 25, pp. 243–254, 2006.

[7] J. Fink and V. Kumar, Online methods for radio signal mapping with mobile robots, *Proceedings of the IEEE International Conference on Robotics and Automation (ICRA)*, pp. 1940–1945, 2010.

[8] S. Eiffert, N. Wallace, H. Kong, N. Pirmarzdashti, and S. Sukkarieh, Resource and response aware path planning for long term autonomy of ground robots in agriculture, *Field Robotics*, Vol. 2, pp. 1–33, 2022.

[9] J. N. Twigg, J. R. Fink, P. L. Yu, and B. M. Sadler, RSS gradient-assisted frontier exploration and radio source localization, *Proceedings of the IEEE International Conference on Robotics and Automation (ICRA)*, pp. 889–895, 2012.

[10] J. Wakulicz, H. Kong, and S. Sukkarieh, Active Information Acquisition under Arbitrary Unknown Disturbances, *Proceedings of the IEEE International Conference on Robotics and Automation*, Vol. 96, pp. 8429–8435, 2021.

[12] J. Lv, X. Zuo, K. Hu, J. Xu. G. Huang, and Y. Liu, Observability-aware intrinsic and extrinsic calibration of LiDAR-IMU systems, *IEEE Transactions on Robotics*, Vol. 38, No. 6, pp. 3734–3753, 2022.

[13] H. Zhang, X. Li, H. Zhong, Y. Yang, Q. M. J. Wu, J. Ge, and Y. Wang, Automated machine vision system for liquid particle inspection of pharmaceutical injection, *IEEE Transactions on Instrumentation and Measurement*, Vol. 67, No. 6, pp. 1278–1297, 2018.

[14] J. Huai, Y. Lin, Y. Zhuang, C. K. Toth, and D. Chen, Observability analysis and keyframe-based filtering for visual inertial odometry with full self-calibration, *IEEE Transactions on Robotics*, Vol. 38, No. 5, pp. 3219–3237, 2022.

[15] J. Wu, M. Wang, Y. Jiang, B. Yi, R. Fan, and M. Liu, Simultaneous hand–eye/robot–world/camera–IMU calibration, *IEEE/ASME Transactions on Mechatronics*, Vol. 27, No. 4, pp. 2278–2289, 2022.

[16] H. Zhang, X. Zhou, H. Zhong, H. Xie, W. He, X. Tan, and Y. Wang, A dynamic window-based UWB-Odometer fusion approach for indoor positioning, *IEEE Sensors Journal*, Vol. 23, No. 3, pp. 2922–2931, 2023.

[17] J. Vallet, O. Kaltiokallio, M. Myrsky, J. Saarinen, and M. Bocca, Simultaneous RSS-based localization and model calibration in wireless networks with a mobile robot, *Procedia Computer Science*, pp. 1106–1113, 2012.

[18] G. Mao, B. Anderson, and B. Fidan, Path loss exponent estimation for wireless sensor network localization, *Computer Networks*, Vol. 51, No. 10, pp. 2467–2483, 2007.

[19] D. Su, T. Vidal-Calleja, and J. V. Miro, Simultaneous asynchronous microphone array calibration and sound source localisation, *Proceedings of the IEEE/RSJ International Conference on Intelligent Robots and Systems (IROS)*, pp. 5561–5567, 2015.

[20] D. Su, T. Vidal-Calleja, and J. Valls Miro, Asynchronous microphone arrays calibration and sound source tracking, *Autonomous Robots*, Vol. 44, pp. 183–204, 2020.

[21] H. Kong and S. Sukkarieh, Suboptimal receding horizon estimation via noise blocking, *Automatica*, Vol. 98, pp. 66–75, 2018.

[22] H. Kong and S. Sukkarieh, Metamorphic moving horizon estimation, *Automatica*, Vol. 97, pp. 167–171, 2018.

[23] D. Su, H. Kong, S. Sukkarieh, and S. Huang, Necessary and sufficient conditions for observability of SLAM-based TDOA sensor array calibration and source localization, *IEEE Transactions on Robotics*, Vol. 37, No. 5, pp. 1451–1468, 2021.

[24] S. Huang and G. Dissanayake, A critique of current developments in simultaneous localization and mapping, *International Journal of Advanced Robotic Systems*, Vol. 13, No. 5, pp. 1–13, 2016.

[25] J. Andrade-Cetto and A. Sanfeliu, The effects of partial observability when building fully correlated maps, *IEEE Transactions on Robotics*, Vol. 21, No. 4, pp. 771–777, 2005.

[26] Z. Wang and G. Dissanayake, Observability analysis of SLAM using Fisher information matrix, *Proceedings of International Conference on Control, Automation, Robotics and Vision*, pp. 1242–1247, 2008.

[27] K. Madsen, H. B. Nielsen, and O. Tingleff, Methods for non-linear least square problems, Lecture notes, Informatics and Mathematical Modelling, *Technical University of Denmark, Society for Industrial and Applied Mathematics*, 2004.

[28] G. Grisetti, R. Kümmerle, C. Stachniss, and W. Burgard, A tutorial on graph-based SLAM, *IEEE Intelligent Transportation Systems Magazine*, Vol. 2, No. 4, pp. 31–43, 2010.

[29] Y. Bar-Shalom, X. R. Li, and T. Kirubarajan, Estimation with applications to tracking and navigation: Theory, algorithms, and software, John Wiley & Sons, Inc., 2004.

[30] B. Siciliano, L. Sciavicco, L. Villani, and G. Oriolo, Robotics: Modeling, planning, and control, Springer, 2009.

[31] A. Coluccia and F. Ricciato, On ML estimation for automatic RSS-based indoor localization, *Proceedings of the IEEE 5th International Symposium on Wireless Pervasive Computing*, pp. 495–502, 2010.

[32] R. Sari and H. Zayyani, RSS localization using unknown statistical path loss exponent model, *IEEE Communications Letters*, Vol. 22, No. 9, pp. 1830–1833, 2018.

[33] Y. I. Wu, H. Wang, and X. Zheng, WSN localization using RSS in three-dimensional space—A geometric method with closed-form solution, *IEEE Sensors Journal*, Vol. 16, No. 11, pp. 4397–4404, 2016.